Chapter-4

Fluorescent CNDs from aqueous extract of Andrographis paniculata and their applications

4.1 Introduction

Andrographis paniculata (AP), also known as "Kalmegh," is a member of the Acanthaceae family. Andrographolide, neoandrographolide, and other phytoconstituents such as stigma sterols, 5, 7, 2′, 3′-tetramethoxy-flavanone, 5-Hydroxy-7, 2′, 3′-trimethoxy-flavanone, etc. are found in the AP plant [Yue *et al*., 2022; Malik *et al*., 2021]. It is a well-known medicinal plant with andrographolide as its main bioactive phytoconstituents. It has been used for centuries in India and other parts of the world for anti-cancer, anti-diabetic, hepato-protective, anti-inflammatory, and anti-oxidant properties [Dai *et al*., 2019].

As discussed in **Chapter 1**, Carbon nanodots (CNDs) are fluorescent carbon nanomaterials with tunable fluorescence that range in size from 1 to 10 nm. Various approaches have been successfully employed for their synthesis. For successful and affordable bioimaging applicability, the CNDs must possess significant biocompatibility, minimal toxicity, *in-vivo* stability, and cost-effective [Đorđević *et al*., 2022].

In this chapter, we present a simple and environmentally friendly hydrothermal method for fabricating multifunctional and fluorescent CNDs using an aqueous extract of fresh AP leaves as the carbon source. The reinforcement of such carbon nanomaterials may enable control of the fundamental properties of various materials, leading to the

development of new biomedical and biochemical devices with unique properties for use in health and industry.

4.2 Experimental section

4.2.1 Materials

DPPH (1, 1-diphenyl-2-picrylhydrazyl), MTT (3-(4, 5-dimethylthiazol-2-yl)-2, 5-diphenyltetrazolium bromide), DAPI (4′,6-diamidino-2-phenylindole), methanol, dichloromethane, formic acid, and quinine sulfate were procured from Sigma-Aldrich Co. LLC. The detailed materials have been provided in chapter **3**.

4.2.2 Fabrication of CNDs from aqueous extract of leaves of *Andrographis paniculata* (AP)

CNDs were fabricated by hydrothermal treatment of an aqueous extract of fresh AP leaves, as shown in Scheme **4.1**. AAPCDs denote carbon nanodots derived from aqueous extract of fresh leaves of AP, whereas AEAP denotes aqueous extract of fresh leaves of AP. In order to prepare AEAP, 10.0 g of fresh leaves were boiled in 150 mL of water until the volume was reduced to 100 mL. The prepared extract was filtered before being placed in a teflon-lined hydrothermal autoclave and heated at 160°C for 8 h. CNDs were centrifuged at 11000 rpm for 15 min after cooling to room temperature and then further purified using a 0.22 μm membrane syringe filter. They were stored at 4^0C for further characterizations and biological evaluations.

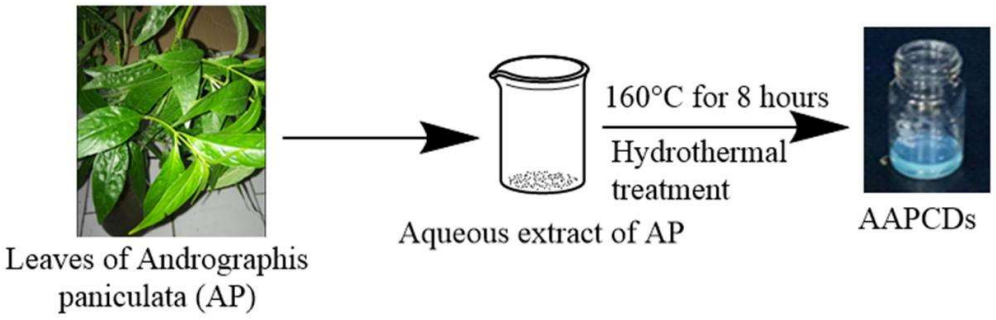

Scheme 4.1. Schematic representation of the formation process of AAPCDs from the fresh leaves of *Andrographis paniculata* by hydrothermal treatment.

4.2.3 Characterization of AAPCDs

The fabricated CNDs have been characterized using different techniques to study their morphology, fluorescence properties, surface functional groups, crystallinity, elemental composition, stability, and quantum yield. The detailed procedures for the metal sensing by AAPCDs are provided in chapter **3**.

4.2.4 Applications of AAPCDs

4.2.4.1 Sensing of environmentally and biologically relevant metal ions

The metal ion sensing ability of the AAPCD was evaluated per the previously reported methods with certain modifications [Edison *et al.,* 2016]. The detailed procedures for the metal sensing by AAPCDs are provided in chapter **3**.

4.2.4.2 Cytotoxicity studies and cellular imaging of AAPCDs

MTT assay was carried out as per the previously reported methods with certain modifications [Pandey *et al*., 2020] using different concentrations of AAPCDs (0, 0.1, 0.2, 0.5, 0.7, 1, 1.5, 2.0, 2.5, 3.0 mg/ mL) employing MCF-7 breast cancer cells. Other

details have been provided in Chapter **3**. For cellular imaging, MCF-7 cells were seeded at a density of 5×10^6 cells per well in a 6-well plate. The cells were then grown for 24 h in a 5% CO_2 humidified incubator at 37°C and were then incubated for another 24 h after being treated with AAPCDs (1.5 mg/mL). The cells were washed three times with 1X PBS before being fixed in 4% paraformaldehyde for 30 min and then counterstained with DAPI for nuclear staining. EVOS invitrogen fluorescence microscopy (Life technologies) was used for *in-vitro* cellular imaging.

4.2.4.3 Viability studies using multidrug-resistant bacterial culture

The viability of MDR clinically isolated strains of *Staphylococcus aureus* (G+) and *Klebsiella pneumonia* (G-) was tested using the disc diffusion method [Torkian *et al*., 2022] with minor modifications with AAPCDs (50µL of 9.6 mg/mL). Other details have been provided in Chapter **3**.

4.2.4.4 Free radicals sensing and scavenging potential

The radical scavenging ability of AAPCDs at different concentrations of 240 µg/mL, 480 µg/mL, and 960 µg/mL was determined using a modified DPPH assay [Sheng *et al*., 2022]. The detailed procedures for the free radical scavenging potential of CNDs are provided in chapter **3**.

4.2.4.5 CNDs as fluorescent ink

Owing to their excellent optical and chemical properties, the fabricated AAPCDs may be suitable for various applications. This ink was used to create filter paper letters AAPCD and other structures. Because the aqueous solution of AAPCDs was used directly, a chemical modification was not needed. Under UV light with a wavelength of 366 nm, this ink could be seen clearly.

4.2.4.6 In-vivo toxicity evaluation

CNDs are expected not to induce severe adverse effects in animals to be used in therapeutic settings. Ethical treatment and housing conditions are provided in Chapter **3**. On day 0, the AAPCDs were dispersed in PBS to make a dispersion with a concentration of 2 mg/kg BW and administered intraperitoneal injection. Mice in the control group were administered with PBS. All experimental animals survived the experiment, and their body weight changes were identical to those of the control group. On the 14th day, blood was obtained from the mice, and routine biochemical and hematological assays were done as described in chapter **3**.

4.2.5 Statistical analysis

The data is presented as Mean± Standard Deviation (SD). The student's t-test was used to perform the statistical studies (GraphPad Prism Version 5.0). $p < 0.05$ was considered as a criterion for significance.

4.3 Results and Discussion

4.3.1 Formation of AAPCDs

Andrographis paniculata leaves were collected from the campus of IIT (BHU) and authenticated by certified taxonomist Prof. N.K. Dubey at the Department of Botany, Banaras Hindu University (BHU), Varanasi, India (Specimen No. Acantha. 2020/1). Figure **4.1** shows a PCR gel image with the matK gene. Based on these observations the plant was authenticated through DNA fingerprinting with a percent identity of 99.67%.

Decomposition, polymerization, aggregations, carbonization, and passivation are all possible mechanisms responsible for CND formation [Hola *et al*., 2017; Song *et al*., 2016; Krysmann *et al*., 2012]. Diterpenes (andrographolide, neoandrographolide), flavonoids (5, 7, 2′, 3′-Tetramethoxy-flavanone, 5-Hydroxy-7, 2′, 3′-trimethoxyflavanone), and stigmasterols are among the phytoconstituents found in AP plant extracts [Rao *et al*., 2004]. Hydroxyl, carboxylic, carbonyl, and lactone groups are present in these compounds, and these chemical moieties can dehydrate under the right hydrothermal conditions [Edison *et al*., 2016]. After the aromatic centers are shaped, the photoluminescence carbon cores are formed. The photoluminescence behavioral characteristics of such fluorescent carbon nanomaterials may be due to interactions between the carbon core and surrounding chemical moieties and hybridization [Zhu *et al*., 2015]. The AAPCDs concentration in aqueous solution was 9.6 mg/mL.

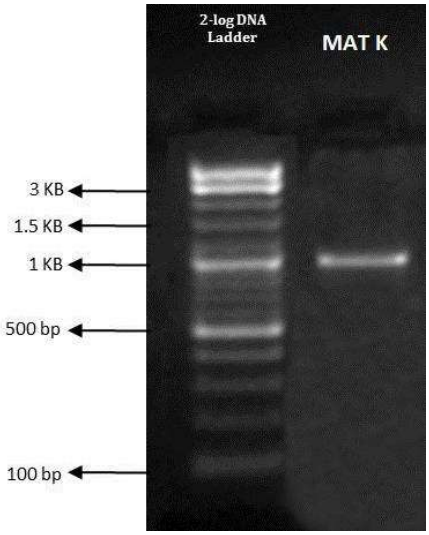

Figure 4.1. PCR gel image with matK gene.

4.3.2 Characterization of AAPCDs

HR-TEM, XRD, TGA, zeta-potential measurements, and FT-IR were used to examine the AAPCDs thoroughly. HR-TEM was used to determine the size of AAPCDs. Figure **4.2 a** depicts the size of the AAPCDs, which range from 8 to 11 nm in diameter with a 9±0.25 nm average diameter. The SAED pattern of AAPCDs, as shown in Figure **4.2 b**, is characterized by a diffused halo devoid of rings, indicating the polycrystalline and amorphous nature of the fabricated CNDs.

The amorphous nature of AAPCDs indicates their proper synthesis. The diffraction peak at 2Θ of 28.23° (Figure **4.2 c**) is attributed to highly disordered carbon atoms and (002) graphite lattice. The peaks correspond to crystal planes (002), (100), (102), and (103) at 28.23°, 40.34°, 50.10°, and 58.64°, respectively. In this case, the first three peaks represent graphite (sp^2), and the last one represents diamond (sp^3). The d-spacing for the planes (002), (100), (102), and (103) was calculated to be 0.31, 0.22, 0.20, and 0.18 nm, respectively, which is similar to graphitic lattice spacing [Chunduri *et al.,* 2016].

As shown in Figure **4.2 d**, FTIR spectra were used to investigate the functional groups and chemical structure of AAPCDs. They exhibited a broad and distinct absorption band of the OH and NH at around 3387 cm^{-1}. The bending and stretching vibrations of C–O bonds in carboxyl groups were represented by the peaks at 1076 cm^{-1} and 1026 cm^{-1}. The C-H and C-N stretching vibration modes could be assigned to the peaks at about 2929 cm^{-1} and 1408 cm^{-1}, respectively. The presence of functional groups is responsible for the AAPCDs' hydrophilicity and stability, as previously stated.

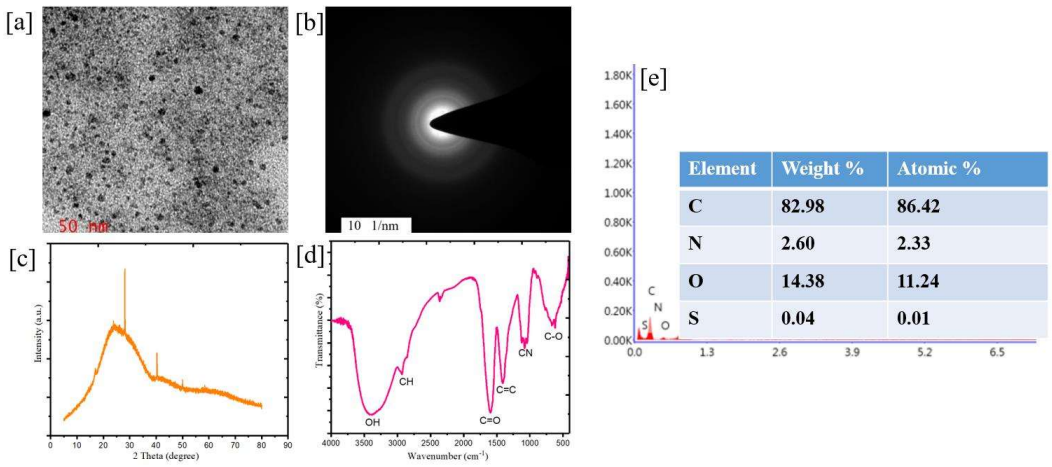

Element	Weight %	Atomic %
C	82.98	86.42
N	2.60	2.33
O	14.38	11.24
S	0.04	0.01

Figure 4.2.Characterization of AAPCDs [a] HR-TEM micrograph [b] Selected area electron diffraction (SAED) patterns [c] XRD Pattern [d] FT-IR Spectrum [e] Energy dispersive x-ray analysis (EDX) spectrum of AAPCDs.

These findings indicated that AAPCDs were associated with carbonyl, carboxylic, and hydroxyl groups during their formation, which could have come from moieties present in the precursor. The elemental abundance and composition of AAPCDs were determined using EDS. The presence of (O) oxygen, (N) nitrogen, and (C) carbon in CNDs was demonstrated by EDS elemental mapping distributions, as shown in Figure **4.2 e**, which can be correlated with the distribution of the various functional groups present on the surface of AAPCDs. These findings revealed that AAPCDs were readily soluble in water due to polar functional groups of O and N on the surface.

AAPCDs were found to have a pH of 6.04. The pH of the fabricated CNDs should be kept within a range that closely resembles physiological values, such as pH 7–8. As a result, incorporating CNDs into appropriate pharmaceutical formulations will be beneficial [Lee *et al*., 2003]

4.3.3 Optical properties of AAPCDs

Since the fluorescence and quantum yield of CNDs are linked to their surface character and surface defects, surface functionalization is of prime importance [Dimos *et al*., 2016]. Effective surface passivation is a critical parameter in the fabrication of high fluorescence yield CNDs [Lim *et al*., 2015]. The UV-vis absorption spectrum of AAPCDs, as shown in Figure **4.3 a**, has a peak at 265 nm, which corresponds to the aromatic ring's π–π* transition. The carbonic core center is responsible for the absorption peak at 265 nm [Xu *et al*., 2014].

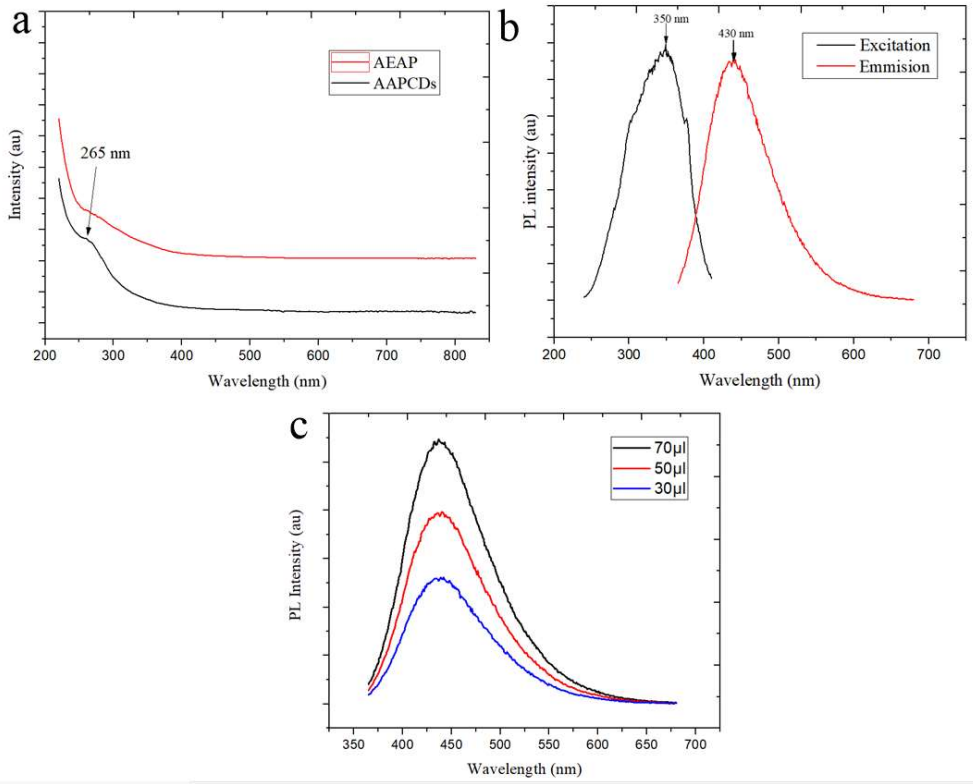

Figure 4.3. Optical properties of AAPCDs [a] UV-visible absorption spectrum [b] Photoluminescent spectra [c] Concentration dependent photoluminescent spectrum at excitation wavelength of 350 nm.

Excitation spectra were used to determine the maximum excitation value found at 350 nm. When excited at 350 nm, the AAPCDs showed fluorescence in the 380-600 nm range, with the maximum at 430 nm, as shown in Figure **4.3 b**. Figure **4.3 c** shows a typical excitation wavelength-dependent spectrum at various AAPCDs concentrations. This could be due to the optical selection of different surface defect states near the Fermi level of CNDs [He *et al*., 2017; Zhu *et al*., 2015]. The CNDs are made up of a carbon core linked to various surface functional groups. The excellent fluorescent aspects of CNDs are due to the π and π* electronic levels corresponding to sp^2 hybrids, which are confined to the band gap of σ and σ* states of the sp^3 surrounding media. Because the excitons in these CNDs have an infinite Bohr diameter, they have a non-zero band gap, illustrating quantum confinement effects and fluorescence emission [Zhu *et al*., 2015; Li *et al*., 2012]. The QY of AAPCDs in an aqueous solution was determined using quinine sulfate as a reference. The quantum yield was measured at 350 nm excitation wavelength and found to be 15.10%. The QY value of AAPCDs was higher than that of most reported non-passivating CNDs. As a result, the fluorescence characteristic of the fabricated AAPCDs has significant research potential. The contribution of hydroxyl groups to the efficient enhancement of intrinsic state emissions by restraining non-radiative electron-hole recombination could explain the improved photoluminescence [Shukla *et al*., 2019].

4.3.4 Stability studies of CNDs

As depicted in Figure **4.4 a**, when these CNDs were irradiated under UV at different time intervals up to 120 min, they were photostable. Weight loss at various temperatures, as shown in thermogram Figure **4.4 b**, demonstrates the thermal behavior and composition of the AAPCDs. TGA spectrum shows the amount and rate of change in

material weight (weight loss) as a function of temperature in a controlled environment with a five-step degradation pattern. This experiment was conducted in a nitrogen environment with a heating rate of 10 °C min^{-1}. At 150 °C, there was an initial 11% weight loss, possibly due to the removal of water molecules and other molecules attached to CNDs via weak hydrogen bonds. Furthermore, weight loss was observed at 225°C (15%), 365°C (33% weight loss), 545°C (51% weight loss), and 768°C (67%) temperatures, which could be due to the decomposition of organic functional groups in AAPCDs, indicating their thermal behavior up to 900°C. Beyond 900 °C, the curve flattened out, and about 15% of AAPCDs remained as the charred carbon. These findings have also been reported in previous reports [Mewada *et al*., 2013; Mehta *et al*., 2014].

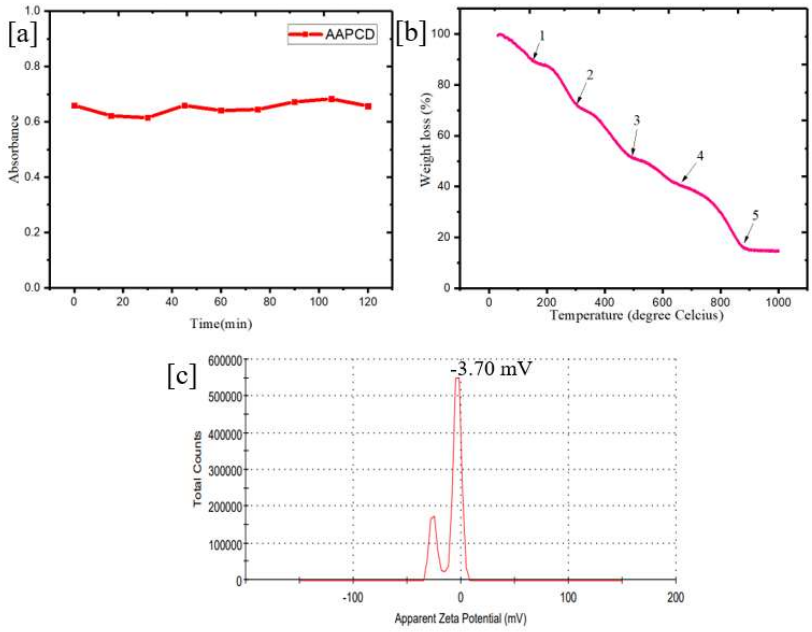

Figure 4.4 Stability studies of CNDs [a] Photostability study under UV illumination at a different time interval up to 120 min [b] Thermo gravimetric analysis spectrum [c] Zeta potential of AAPCD.

The zeta potential (ZP) is the potential in the slipping/shear plane of a colloid particle moving under an electric field, and it can be used to predict particle agglomeration. The AAPCDs' zeta potential in aqueous media was -3.70 mV, as shown in Figure **4.4 c**, which could be due to the presence of various carbonyl, carboxyl, and hydroxyl groups on the CNDs' surface. In this case, the AAPCDs with negative surface charges tend to repel each other, preventing the particles from aggregating. Overall, the fabricated CNDs can remain stable for several months without using any surfactant agents due to the repellent columbic force [Singh *et al*., 2019]. The ZP of -30 mV to +30 mV is thought to have enough repulsive force to achieve better physical colloidal stability [Bhattacharjee *et al*., 2016].

4.3.5 Applications of AAPCDs

AAPCDs have demonstrated utility in various biomedical and pharmaceutical domains such as metal sensing, bio-imaging, free radicals sensing and scavenging, and fluorescent ink.

4.3.5.1 Metal sensing

Selectivity is a critical criterion for evaluating a CNDs' performance. Thus, we investigated the differences in fluorescence emission intensity by adding various biologically and environmentally relevant metal ions to AAPCDs at a concentration of 250 µM, including Hg^{2+}, Fe^{3+}, Ba^{2+}, Cu^{2+}, Ca^{2+}, K^{+}, Na^{+}, NH^{4+}, As^{3+}, Bi^{3+}, and Pb^{2+} obtaining the corresponding fluorescence emission spectra (Figure **4.5 a**). Fe^{3+} had the most considerable propensity to quench the fluorescence intensity of AAPCDs among the metal ions.

A sensitivity titration was also carried out at various Fe^{3+} concentrations ranging from 0 to 250 µM. The emission of the AAPCDs at 450 nm steadily declined as the concentration of Fe^{3+} increased, as shown in Figure **4.5 b**; this demonstrates that the current sensing system is susceptible to Fe^{3+}. The relationship between F_0/F and Fe^{3+} concentration is shown in the inset. Figure **4.5 c** shows a good linear relationship between the linear ranges at 60–120 µM, with a correlation coefficient (R^2) of 0.986. The LOD was discovered to be 1.9 µM.

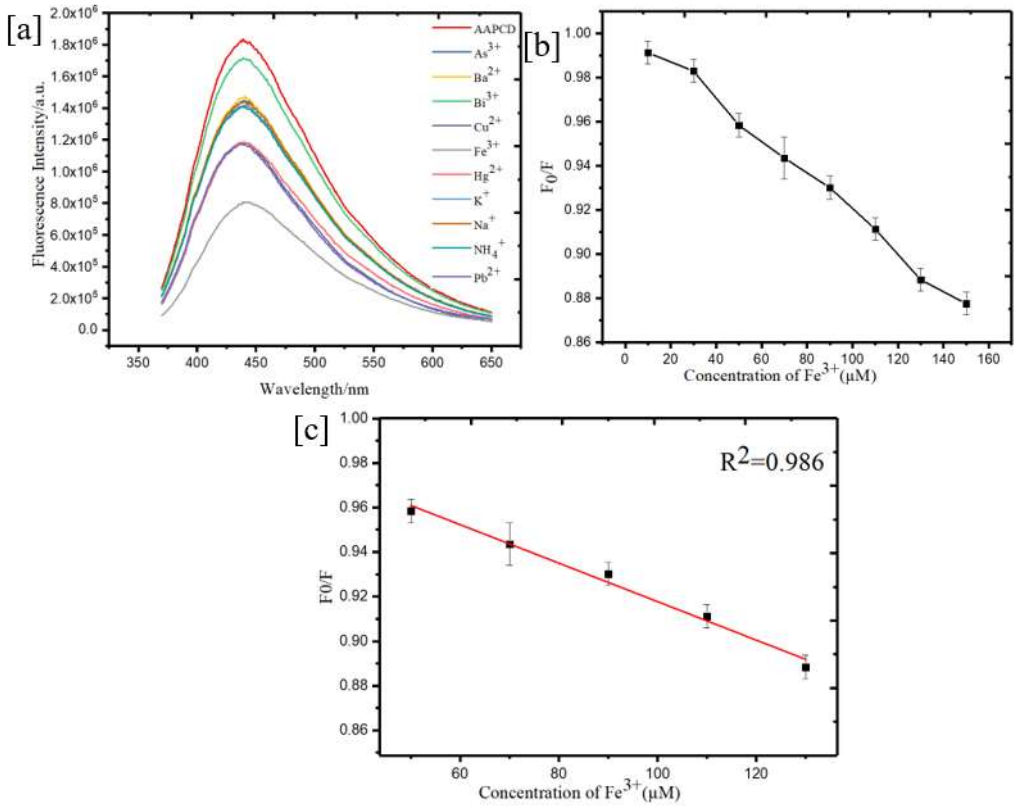

Figure 4.5. Fluorescence sensing of metal ions using AAPCDs. [a] Fluorescence responses of AAPCDs toward various metal ions. The control represents the fluorescence response of the CNDs without any ion. [b] and [c] Fluorescence responses of the AAPCDs in the presence of different concentrations of Fe^{3+}.

For Fe^{3+} sensing, ground-state complex formation, collision quenching, excited-state reaction, molecule rearrangement, and energy transfer are intermolecular interactions responsible for fluorescence quenching [Kumar *et al*., 2017; Zhao *et al*., 2019]. Static quenching and dynamic quenching are two types of quenching mechanisms. The electron transfers from excited AAPCDs to half-filled 3d orbitals of Fe^{3+} caused strong non-radiative electron/hole recombination, resulting in aggregation-induced emission quenching [Khan *et al*., 2019; Wang *et al*., 2017], indicating that Fe^{3+} ions bind to the functional groups on the surface of AAPCDs to form Fe^{3+} chelates. As a result of the coordination of Fe^{3+} on the surface of AAPCDs with nitrogen-bearing groups, carboxyl, and hydroxyl, the radiation transition is destroyed, and fluorescence quenching occurs [Khan *et al*., 2019; Zhao *et al*., 2019].

4.3.5.2 Cytotoxicity and bioimaging studies

Using MCF-7 cells as a model, the MTT assay was employed to assess the cytotoxicity of AAPCDs. As shown in Figure **4.6 a**, cell viability was measured after cells were exposed to various concentrations of AAPCDs, indicating that the AAPCDs had low cytotoxicity up to a specific dose after 24 h of incubation 50% viability at a concentration of 2.0 mg/mL. In the bright field image of the treated MCF-7 cells (Figure **4.6 b**), the morphology of the cells was disrupted, and apoptotic-like bodies were formed compared to the non-treated MCF-7 cells. AAPCDs doses ranging from 0 to 0.7 mg/mL exhibited good cell viability, but as the dose was increased, AAPCDs had cytotoxic effects on cells. As a result, a higher dose of AAPCDs could be used to inhibit cancerous growth, but more in-depth studies are needed. MCF-7 cells with and without AAPCDs treatment are shown in Figure **4.6 b**. AAPCDs-treated cells displayed green fluorescence,

as shown in Figure **4.6 b**. When the nucleus was stained with DAPI (4′,6-diamidino-2-phenylindole), it was revealed that the AAPCDs were mostly found in the cytoplasm, with no fluorescence in the nucleus. Through Figure **4.6 b**, we demonstrate how the fluorescence signal can be monitored in the green spectral region, in contrast to the blue-fluorescing (DAPI) stain, which is well known to bind to DNA strongly.

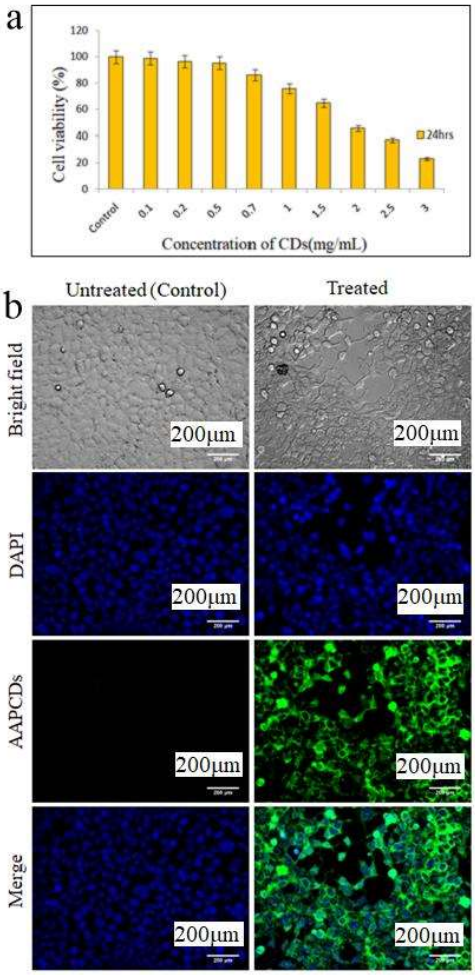

Figure 4.6. Cytotoxicity assay and bioimaging of MCF-7 Cells. [a] Cell viability of MCF-7 human breast cancer cells after incubation with AAPCDs for 24 h, determined by MTT assay [b] Cellular imaging of MCF-7 breast cancer cells under a bright field, blue field (DAPI), green field (AAPCDs) and merge (AAPCDs/DAPI) after 24 h AAPCDS treatment. Scale bar: 200 µm.

The cytoplasm targeting AAPCDs was further confirmed when the emission from the AAPCDs and DAPI were merged. There was no fluorescence in the control cells that had not been treated with AAPCDs.

4.3.5.3 AAPCDs as free radical sensors and scavengers

Using the DPPH as a model, the radical scavenging potential of fabricated AAPCDs was investigated. Upon acceptance of hydrogen radical, DPPH was converted into a stable DPPH-H complex, changing the color of the solution from deep violet to light yellow. By comparing absorbance at 515 nm to the blank, the remaining DPPH was determined.

The dose-dependent scavenging of DPPH radicals by AAPCDs at various concentrations was investigated, as shown in Figure **4.7 a**. After increasing the concentration of AAPCDs, it was discovered that the absorbance of DPPH decreased. The fluorescence of the AAPCDs was effectively quenched after addition to methanolic DPPH solution, as shown in Figures **4.7 b** and **4.7 d**, as determined by fluorescence emission spectra. However, as a control, no quenching in the fluorescence of AAPCDs was observed when methanol was used, as shown in Figure **4.7 c**. As a result, AAPCDs can also be used as free radical probes. CNDs with surface functionalization are excellent electron acceptors and donors. The quenching of AAPCDs fluorescence could be caused by these electron acceptors or donors [Lin *et al.,* 2012; Sachdev *et al*., 2015]. The quenching phenomenon can be seen with the naked eye in Figure **4.7 d**. This could be due to a combination effect between the functional groups on the surface of CNDs and free radicals, which causes the quenchers to break or recombine. According to various reports, CNDs have a good surface-to-volume ratio because their size is less than 10 nm, and they have a variety of

functional groups on their surface. CNDs demonstrate photo-induced electron and energy transfer properties as an acceptor or donor at the same time [Lin *et al.,* 2012; Sachdev *et al*., 2015].

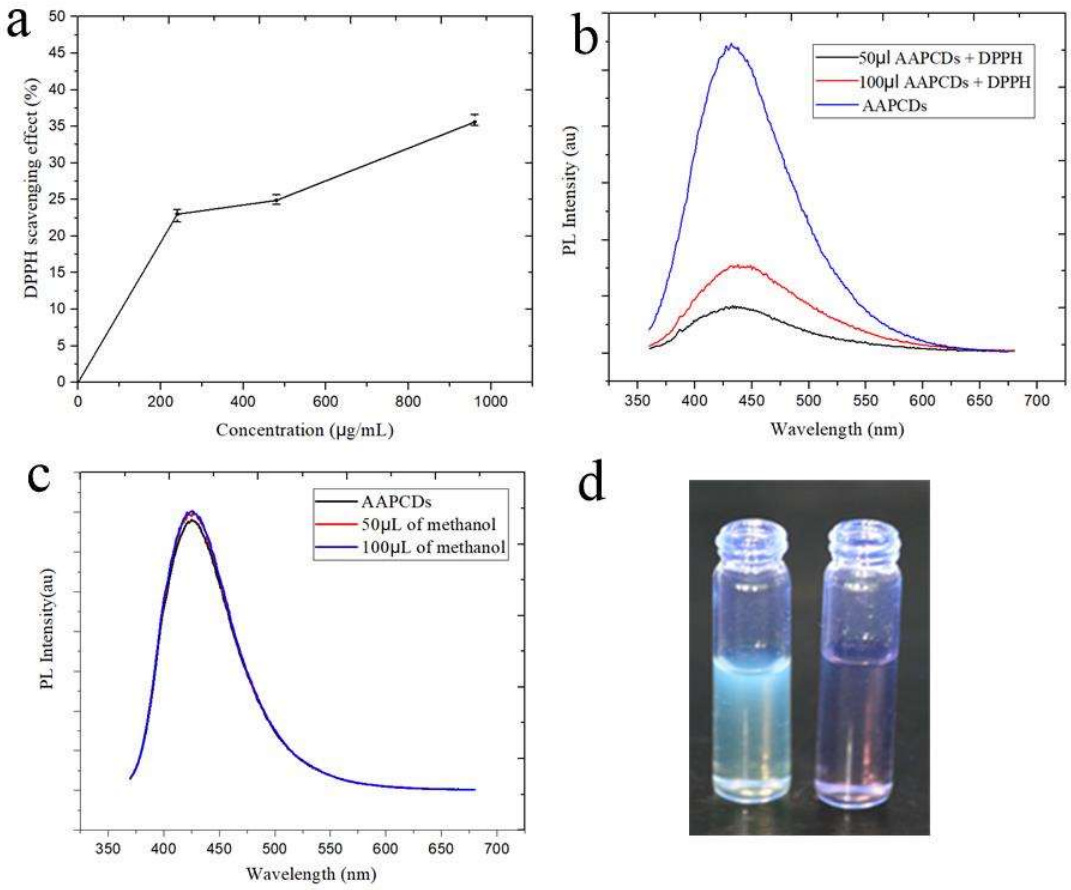

Figure 4.7. Free radicals sensing and scavenging potential. [a] % DPPH scavenging activity for various concentrations of AAPCDs (240 µg/mL, 480 µg/mL & 960 µg/mL) in DPPH-methanol solution [b] Photoluminescent spectra of AAPCDs showing quenching of fluorescence upon addition of free radicals [c] Photoluminescent spectra of AAPCDs upon addition of methanol as a control [d] AAPCDs solution without DPPH (left) and AAPCDs upon addition of DPPH (Right).

In the case of CNDs, dynamic or static quenching may be the cause of fluorescence quenching. Collisions cause dynamic quenching, whereas static quenching occurs when a link forms between the quencher and the fluorophore. Because of the interaction between the structure of DPPH and the surface functional groups of AAPCDs, the fluorescence of AAPCDs was quenched when DPPH was added. The formation of strong hydrogen bonds between AAPCDs and DPPH causes quenching. The quenching phenomenon, in this case, is thought to be caused by the FRET (non-radioactive resonance energy transfer) mechanism [Wang *et al*., 2015; Gong *et al*., 2015].

4.3.5.4 Viability studies with MDR bacterial strains

The viability of MDR clinically isolated strains of *Staphylococcus aureus* (G+) and *Klebsiella pneumonia* (G-) was investigated by treating with AAPCDs. AAPCDs showed no zone of inhibition when compared to ciprofloxacin as a positive control, as shown in Figures **4.8 a** and **4.8 b**. These tests were carried out three times. The findings show that AAPCDs are biocompatible in bacterial cells and can be used in microbiology experiments and bioimaging.

4.3.5.5 AAPCDs as fluorescent ink

Under UV light, the AAPCDs solution fluoresces bright blue and can thus be used as fluorescent ink, as shown in Figure **4.9**. The ink on these CNDs is transparent, biocompatible, non-toxic, and eco-friendly. As a result, synthesized CNDs can be used as a new type of fluorescent ink for security purposes.

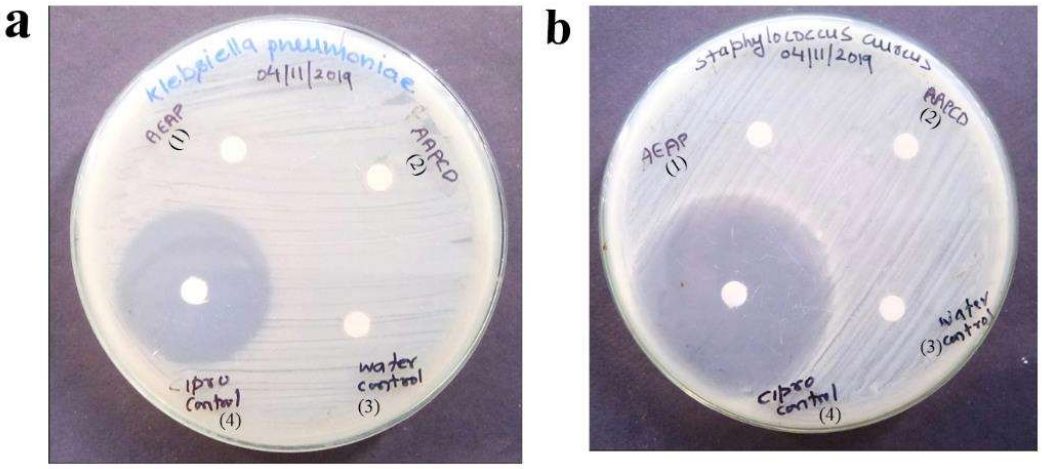

Figure 4.8. Biocompatibility studies on MDR bacterial cells show zones of inhibition [a] *Klebsiella pneumonia* [b] *Staphylococcus aureus* (1) AEAP represent aqueous extract of *Andrographis paniculata*, (2) AAPCDs represent *Andrographis paniculata* derived CNDs, (3) water was used as a control and (4) ciprofloxacin was used as a positive control.

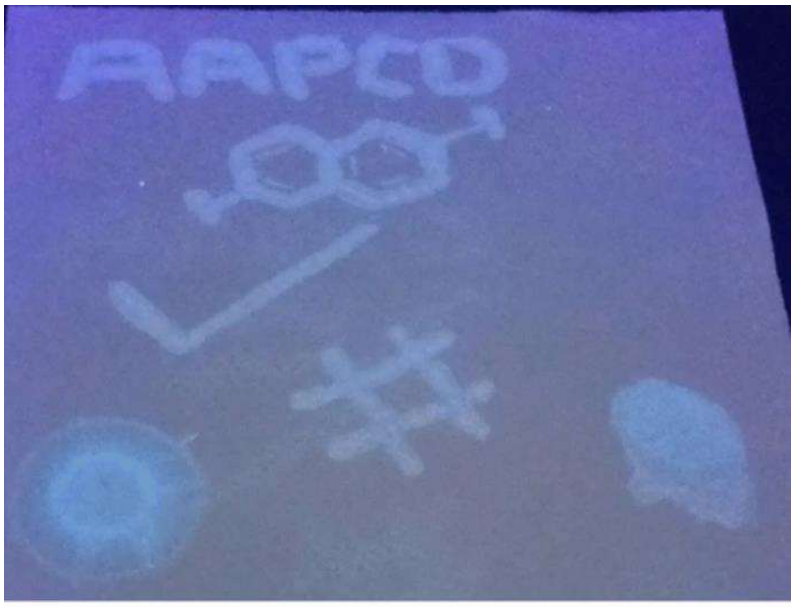

Figure 4.9. AAPCDs formed fluorescent images captured at 366 nm excitation.

4.3.5.6 In-vivo toxicity evaluation in Swiss albino mice

The results showed no evident differences between AAPCDs and control groups. No statistically significant ($p > 0.05$) differences were observed on day 14 of the treatment in any experimental groups; this could be due to the body's immunological regulation. All biochemical assay values were within normal ranges, as shown in Table **4.1**.

Hematology

Peripheral blood was collected from mice post-treatment for hematological toxicity determination and subjected to several hematological parameters evaluation. All the treatment and the normal control groups' values were within the normal range (Table **4.2**). In addition, biochemical parameters such as alanine aminotransferase (ALT), creatinine (CRE), aspartate transaminase (AST), alkaline phosphatase (ALP), blood urea nitrogen (BUN), total bilirubin (TB), cholesterol, and creatine phosphokinase (CPK) were also analyzed to measure organ toxicity as per standard protocols. Biochemical indicators were also within normal limits, showing that the mice were not harmed by delivering AAPCDs.

The histological investigation determined the microscopic interactions between CNDs and biological tissues. There were no evident histopathological changes in the heart, brain, kidney, spleen, lung, or liver observed compared to the control group, as shown in Figure **4.10**. A histopathological examination revealed no signs of severe toxicity. These alterations could be attributable to environmental causes, like the mice in the control group exhibit comparable symptoms. The cells and structure of these organs' samples were confirmed to be normal, and no specific lesion that differed from the control group

was observed. The vital organs' H&E staining revealed the same characteristics as control sections.

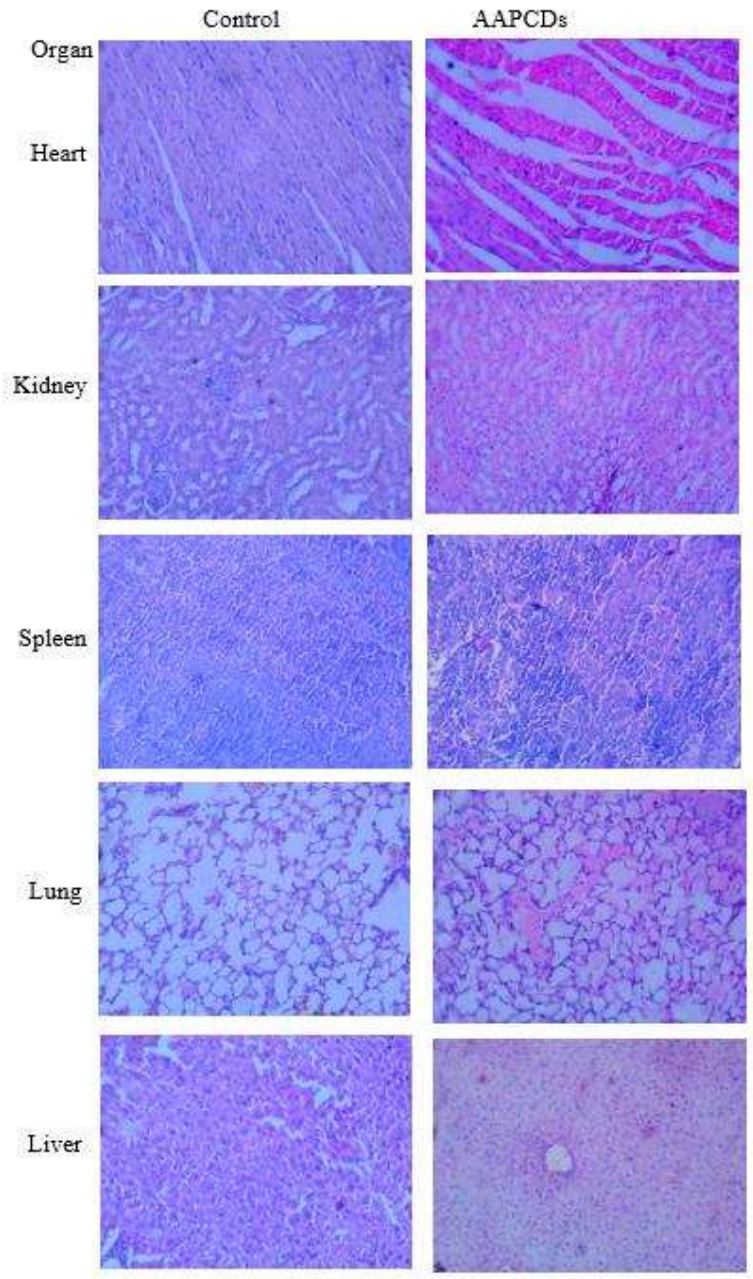

Figure 4.10. Histopathology of different mice organs treated with AAPCDs and control.

On histological evaluation, the heart, kidney, brain, spleen, lung, and liver did not reveal any signs of toxicity, as shown in Figure **4.10**. In the test groups, no evident histological abnormalities or lesions were seen. The test group's cardiac muscle fibers were uniform and normal in shape and size.

Table 4.1. Biochemical parameters of mice treated with AAPCDs and control groups.

Parameters	**Normal Control**	**AAPCDs**
ALP (U/L)	105.13± 5.57	102.06± 4.70
AST(U/L)	134.46± 3.80	134.5± 3.55
ALT(U/L)	51.6± 1.75	55.36± 2.85
Creatinine (mg/dL)	0.23± 0.02	0.22± 0.01
Urea (mg/dL)	40.52± 3.86	42.49± 3.25
Cholesterol (mg/dL)	103± 5.09	99.33± 6.18
Tryglyceride (mg/dL)	106.53± 3.61	108.79± 7.64
Protein (g/dL)	6.39± 0.54	6.40± 0.65
Glucose (mg/dL)	140.93± 9.12	137.9± 3.63
CPK Total(U/L)	96.33± 5.24	101.66 ± 4.78

(Data was represented as mean± SD)

The hepatocytes in the liver samples were normal, and no evidence of inflammation was seen. In the renal portion, the glomerulus structure was normal in texture. There was no evidence of necrosis in any of the histopathological samples examined. There was no steatosis, necrosis, or hydropic degeneration in the exposed hepatic sections. The liver lobule structure was normal, with only a few collagen fibers in the central vein and portal area. The red and white pulps were clear, and the splenic capsule was complete. The

architecture of the lungs was normal, and no inflammation was discovered. The glomerular structure may be seen clearly in portions of the kidneys. Every other day, body weights were measured, and there were no differences between the experimental and control groups.

Table 4.2. Hematological parameters of mice treated with AAPCDs and control groups.

Parameters	**Normal control**	**AAPCDs**
WBC (10^3/μL)	36.54±2.35	36.57±1.62
HGB (g/dL)	11.74±0.64	12.02±0.55
RBC (10^6/μL)	8.27±0.33	8.12±0.42
HCT (%)	36.12±1.40	37.21±1.84
MCV (fL)	45.69±1.03	45.47±1.01
MCH(pg)	14.38±0.21	14.45±0.32
NEUT (%)	55.80±2.94	54.37±6.30
LYM (%)	41.12±5.61	40.25±4.01
MONO (%)	3.76±0.33	3.68±0.40
EO (%)	0.80±0.03	0.81±0.02
BASO (%)	0.02±0.02	0.02±0.01

(Data was represented as mean± SD)

4.4 Conclusions

In this objective, we have demonstrated a simple and environmentally friendly synthesis method to synthesize multifunctional fluorescent CNDs using aqueous extract of *Andrographis paniculata*, as a cheap and readily available carbon source. The CNDs displayed outstanding overall performance, including brilliant optical properties, fine photochemical properties, and thermal stability. Furthermore, the synthesized CNDs have Fe^{3+} ion sensing, bio-labeling, biocompatibility, radical sensing, and favorable free radical scavenging properties, making them promising candidates for various biomedical and environmental applications. We further tested the toxicity of these CNDs in swiss albino mice, and found that they were safe, as evidenced by biochemical, haematological, and histological parameters. Overall, the AAPCD attributes indicate that these environmentally friendly carbon nanomaterials could be prepared on a large scale without using toxic chemicals that are harmful to the environment, opening up many possibilities in biomedical and bioengineering technologies.